

Experimental study on Re number effects on aerodynamic characteristics of 2D square prisms with corner modifications

Xinrong Wang and Ming Gu*

State Key Laboratory for Disaster Reduction in Civil Engineering, Tongji University, Shanghai 200092, China

(Received June 4, 2015, Revised April 8, 2016, Accepted April 11, 2016)

Abstract. Simultaneous pressure measurements on 2D square prisms with various corner modifications were performed in uniform flow with low turbulence level, and the testing Reynolds numbers varied from 1.0×10^5 to 4.8×10^5 . Experimental models were a square prism, three chamfered-corner square prisms ($B/D=5\%$, 10% , and 15% , where B is the chamfered corner dimension and D is the cross-sectional dimension), and six rounded-corner square prisms ($R/D=5\%$, 10% , 15% , 20% , 30% , and 40% , where R is the corner radius). Experimental results of drag coefficients, wind pressure distributions, power spectra of aerodynamic force coefficients, and Strouhal numbers are presented. Ten models are divided into various categories according to the variations of mean drag coefficients with Reynolds number. The mean drag coefficients of models with $B/D \leq 15\%$ and $R/D \leq 15\%$ are unaffected by the Reynolds number. On the contrary, the mean drag coefficients of models with $R/D=20\%$, 30% , and 40% are obviously dependent on Reynolds number. Wind pressure distributions around each model are analyzed according to the categorized results. The influence mechanisms of corner modifications on the aerodynamic characteristics of the square prism are revealed from the perspective of flow around the model, which can be obtained by analyzing the local pressures acting on the model surface.

Keywords: wind tunnel test; 2D square prism; corner modification; aerodynamic characteristic; Reynolds number effect

1. Introduction

The square prism is a common and basic shape widely used in civil engineering structures, such as tall buildings, high-rise structures, and bridge towers. The aerodynamic characteristics of a square prism have received considerable attention in wind engineering. In the past decades, many experimental studies (Vickery 1966, Lee 1975, Okajima 1982, Igarashi 1984, Nakamura and Ohya 1984, Nakamura and Ozono 1987, Knisely 1990, Norberg 1993, Tamura and Miyagi 1999, Huang *et al.* 2010, Huang and Lin 2011, Yen and Yang 2011) have been conducted to investigate its aerodynamic characteristics, including the surface pressure distributions, the aerodynamic forces, the vortex shedding, and the wake characteristics. These studies showed that the aerodynamic characteristics of a square prism are unaffected by the Reynolds number, but obviously influenced by the wind attack angle. Flow visualization experiments conducted by Igarashi (1984) investigated the flow characteristics around a square prism in the attack angle range of $0^\circ \leq \theta \leq 45^\circ$.

*Corresponding author, Professor, E-mail: minggu@tongji.edu.cn

The results showed that the separated flow was symmetrical in the attack angle range of $0^\circ \leq \theta \leq 5^\circ$, but asymmetrical in the attack angle range of $5^\circ < \theta \leq 13^\circ$. For the attack angle range of $14^\circ - 15^\circ \leq \theta \leq 45^\circ$, the separated flow reattached to the side surface of the model exposed to wind. Yen and Yang (2011) utilized the particle image velocimetry method to analyze the flow structure, wake-flow characteristics, and aerodynamic force coefficients of a square prism at various Reynolds numbers ($4 \times 10^3 < Re < 3.6 \times 10^4$) and attack angles ($0^\circ < \theta < 45^\circ$). The results revealed that the lift coefficient was unaffected by the Reynolds number. Moreover, the maximum lift coefficient occurred at $\theta = 13^\circ$, whereas the minimum drag coefficient occurred at $\theta = 12^\circ$. In general, previous experimental results provided a comprehensive understanding of the aerodynamic characteristics of a square prism. Many numerical studies (Okajima 1990, Tamura *et al.* 1990, Yu and Kareem 1996, 1997, Bosch and Rodi 1998, Tamura *et al.* 1998, Sohankar *et al.* 2000, Shimada and Ishihara 2002, Oka and Ishihara 2009) have also been conducted to analyze the aerodynamic characteristics of a square prism. These studies provided a more detailed understanding of flow around a square prism.

Corner modifications for tall buildings have become the major aerodynamic measures commonly used in design practice. Some studies (Kwok 1988, Hayashida and Iwasa 1990, Miyashita *et al.* 1993, Tamura *et al.* 1998, Tamura and Miyagi 1999, Wang *et al.* 2003, Choi and Kwon 2003, Gu and Quan 2004, Carassale *et al.* 2013, 2014) have verified that the introduction of appropriate corner modifications can obviously decrease the along-wind and cross-wind loads on tall buildings. Tamura *et al.* (1998, 1999) investigated the effects of chamfered corners and rounded corners on the aerodynamic characteristics of a square prism by combining the numerical simulation results with the experimental results. The results showed that chamfered and rounded corners decreased the drag force of a square prism because of the reduction in wake width. Furthermore, even when the wind attack angle is $\theta = 0^\circ$ the separated flow reattached to the side surfaces of the square prism with $R/D = 1/6$. Carassale *et al.* (2013, 2014) conducted wind tunnel tests to measure the aerodynamic forces and wind pressures acting on the square prisms at various Reynolds numbers ($1.7 \times 10^4 \leq Re \leq 2.3 \times 10^5$) and attack angles ($0^\circ < \theta < 45^\circ$). The experimental models were a square prism and two rounded-corner models ($R/D = 1/15$ and $2/15$). The introduction of rounded corners reduced the critical angle of incidence for which the flow reattached to the lateral face exposed to wind. Moreover, for the rounded-corner model with $R/D = 2/15$, two flow regimes were found around the model in turbulent flow, and the transition between these two regimes were governed by the Reynolds number. Appropriate corner modifications are beneficial because they can reduce design wind loads and building motions. However, corner modifications may produce more complex flow around the body. Thus, determining the influence mechanisms of corner modification on the aerodynamic characteristics of the model is difficult. In addition, corner shapes for tall buildings have diverse forms, and the effects of different corner shapes on the aerodynamic characteristics of tall buildings also differ. Therefore, systematically investigating some typical corner modifications on the aerodynamic characteristics of typical building models is necessary.

The aerodynamic characteristics of square prisms with corner modifications may be influenced by the Reynolds number, which needs to be further investigated. For a square prism, the flow separation location is fixed and its aerodynamic characteristics are unaffected by the Reynolds number. For a circular prism, the flow separation location is dependent on the Reynolds number, and its aerodynamic characteristics are obviously influenced by the Reynolds number. Thus, for prisms between the two cases, such as square prisms with various rounded corners, the Reynolds number effects on their aerodynamic characteristics could be limited. This is related to the absence

of fixed separation points and the formation of the separated shear layer at the leading edge. Several studies (Carassale *et al.* 2013, 2014) have shown that various flow regimes were found around the square prism with the rounded corner of $R/D = 2/15$, and the transition between these regimes were governed by the Reynolds number. However, no systematical studies have been performed to investigate the Reynolds number effects on the aerodynamic characteristics of square prisms with various rounded corners. Thus, this topic is one of the focuses of the present study.

Previous studies on the aerodynamic characteristics of a square prism are comparatively comprehensive. Many studies on the effects of corner modifications on the aerodynamic characteristics of a square prism are also available. As a complement to the previous studies, wind pressures acting on square prisms with various corner modifications are obtained in the present study by simultaneous pressure measurements in low turbulence uniform flow for the Reynolds number ranging from 1.0×10^5 to 4.8×10^5 . The testing models are a square prism, three chamfered-corner square prisms ($B/D=5\%$, 10% , and 15%), and six rounded-corner square prisms ($R/D = 5\%$, 10% , 15% , 20% , 30% , and 40%). The experimental results of wind pressure distributions, mean drag coefficients, power spectra of aerodynamic force coefficients, and Strouhal numbers for these models are discussed. The influence mechanisms of corner modifications on the aerodynamic characteristics of a square prism are revealed from the perspective of the variations of flow around the model. The extent of the Reynolds number effects on the aerodynamic characteristics of each model is analyzed. Accordingly, the sensitivity limit to the Reynolds number is determined for square prisms with various corner modifications.

2. Experimental details

2.1 Experimental setup

The experiments were performed in a closed-circuit wind tunnel at Tongji University. The cross section of this tunnel is 3 m wide and 2.5 m high. The test model was supported by a steel frame mounted at the center of the tunnel cross-section. Fig. 1 shows the photograph of the test setup and model. The steel frame had sufficient strength and rigidity to ensure experimental accuracy under the condition of high wind speed. End plates were installed at the extremities of the model to produce the 2D flow around the testing model, and the validation of the 2D flow around the testing model was given by Wang and Gu (2015). End plates were made of 8 mm-thick aluminum to meet the test requirements of strength and rigidity. The leading edges of end plates were chamfered to decrease the width of the wake flow, thereby reducing the influence of wake flow on the testing models. The size of the end plates is shown in Fig. 2. The DSM3000 electronic pressure scan valve system was used to measure the wind pressures acting on the models. The sampling frequency was 312.5 Hz, and the measuring duration was 28.8 s.

2.2 Test models and conditions

2D square prisms with various corner modifications were adopted, as shown in Fig. 3. Apart from a square prism, square prisms with three kinds of chamfered corners ($B/D=5\%$, 10% , and 15%) and six kinds of rounded corners ($R/D= 5\%$, 10% , 15% , 20% , 30% , and 40%) were also adopted for this study, as shown in Table 1. The chamfered corner ratio B/D refers to the ratio of the chamfered corner dimension B to the model dimension D , and the rounded corner ratio R/D

refers to the ratio of the corner radius R to the model dimension D . The length L and the model dimension D of ten models were 1.5 and 0.2 m, respectively. Therefore, the aspect ratio was 7.5 and the blockage ratio was 4%. All models were symmetrical in both the streamwise direction and the vertical axis. The pressure taps were arranged around the model surface at the midspan. Using three models as examples, the arrangements of the pressure taps at the midspan are shown in Fig. 3. All models were made of 7 mm-thick organic glass to maintain smooth and flat surfaces. The pressure measurements were corrected for the pressure signal distortion, both in magnitude and phase, because of the pneumatic tubing with 0.5 mm internal diameter and 0.8 m length.

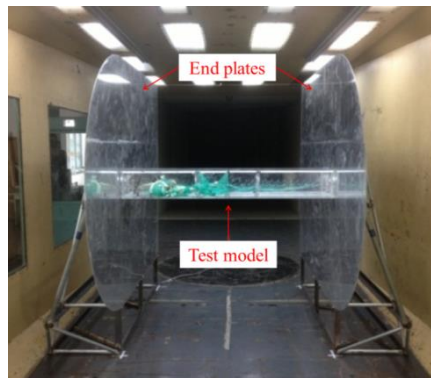


Fig. 1 Wind tunnel test model

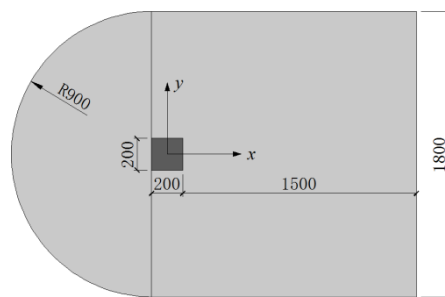


Fig. 2 Size of the end plate (units: mm)

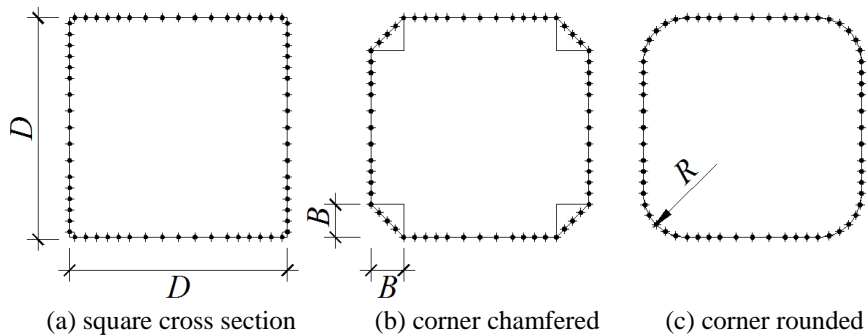


Fig. 3 Sketch of corner modifications and arrangements of pressure taps

Table 1 Experimental models

Model type	<i>B/D</i> or <i>R/D</i>
Square prism	0%
Chamfered-corner models	5%, 10%, and 15%
Rounded-corner models	5%, 10%, 15%, 20%, 30%, and 40%

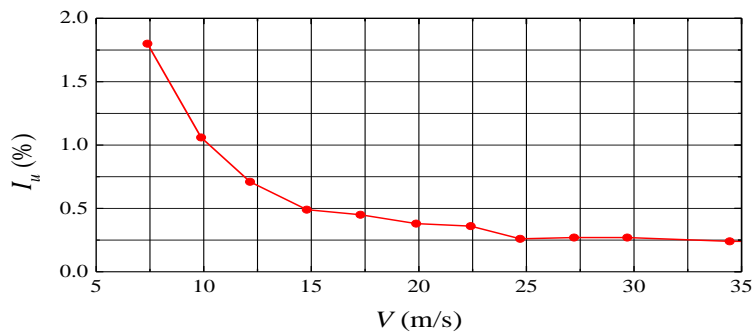


Fig. 4 Variation of the longitudinal turbulence intensity with the mean wind speed

The incoming flow was uniform flow with low turbulence level. Fig. 4 presents the variation of the longitudinal turbulence intensity at the model location with the mean wind speed. The longitudinal turbulence intensity was approximately 1% when the wind speed reached 10 m/s, and was less than 0.5% when the wind speed exceeded 15 m/s. The testing wind speed ranged from 7.5 m/s to 35 m/s, and the testing Reynolds numbers were from 1.0×10^5 to 4.8×10^5 accordingly.

3. Data processing methods

The time history of the wind pressure coefficients at pressure tap *i* is calculated as follows

$$C_p(i, t) = \frac{p_i - p_\infty}{(1/2)\rho U^2} \tag{1}$$

where p_i is the actual pressure measured at the pressure tap *i*; p_∞ is the reference static pressure, which is the static pressure in the upstream of the model; ρ and U are the air density and wind velocity, respectively. Aerodynamic forces (drag and lift) are obtained by integrating the wind pressures around the model surface (neglecting viscous drag).

$$C_D(t) = \frac{F_x(t)}{(1/2)\rho U_0^2 D} = \frac{1}{D} \sum_i C_p(i, t) \cdot \Delta S_i \cdot \cos \theta_i \tag{2}$$

$$C_L(t) = \frac{F_y(t)}{(1/2)\rho U_0^2 D} = \frac{1}{D} \sum_i C_p(i, t) \cdot \Delta S_i \cdot \sin \theta_i \tag{3}$$

where D is the across-wind dimension; ΔS_i represents the width on the model surface belonging to

the pressure tap i ; θ_i is the angle between the wind pressure direction and the incoming flow direction (see Fig. 5).

The Strouhal number is defined as follows

$$St = f \cdot D/U \quad (4)$$

where f is the frequency corresponding to the obvious peak in the power spectrum of lift force.

4. Experimental results

4.1 Previous data for validation

Table 2 compares the aerodynamic parameters of the square prism obtained by the present experiments with those of previous experimental and numerical studies (Lee 1975, Naudascher *et al.* 1981, Tamura and Kuwahara 1990, Norberg 1993, Lyn *et al.* 1995, Murakami and Mochida 1995, Koutmos and Mavridis 1997, Taylor and Vezza 1999, Nishimura and Taniike 2000). These parameters are mean drag coefficients, mean lift coefficients, and Strouhal numbers. The present results are in the variation range of the previous results. Fig. 6 compares the wind pressure distributions around the model surface at $Re \approx 3.4 \times 10^5$ with the previous results (Pocha 1971, Lee 1975, Otsuki *et al.* 1978, Bearman and Obasaju 1982, Nishimura and Taniike 2000, Ono and Tamura 2001, Oka and Ishihara 2009, Cao *et al.* 2014). In Fig. 6(a), for the mean pressure coefficients on the windward side of the model, no differences are found between the present results and the previous data. For the mean pressure coefficients on the side surfaces and the leeward side, obvious differences are observed for the previous results; the present results are in good agreement with the experimental results of Nishimura and Taniike (2000). In Fig. 6(b), fluctuating pressure distributions on the windward side of the model are nearly the same for various previous studies; the present results agree well with the results of these studies. For the fluctuating pressure distributions on the side surfaces and leeward side, obvious differences are observed for various previous studies; the present results are a slightly smaller than the results of these studies.

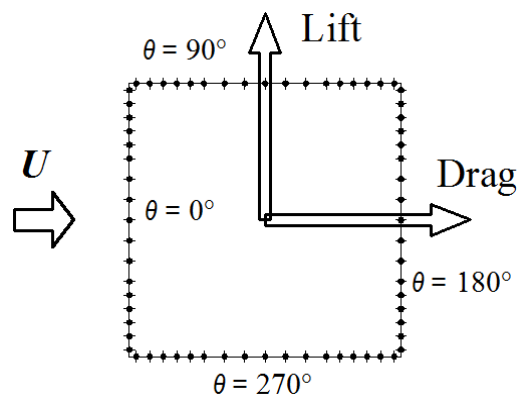


Fig. 5 Sketch of the drag and lift force

Table 2 Comparison of aerodynamic parameters for a square prism

Authors	Re	$C_{D\ mean}$	$C_{L\ mean}$	St
Present results	$1.0 \times 10^5 - 4.8 \times 10^5$	2.19–2.25	0	0.138
Nishimura and Taniike (exp. 2000)	4×10^4	2.33	0	0.126
Lee (exp. 1975)	1.76×10^5	2.04	0.021	0.1214
Norberg (exp. 1993)	5×10^3	2.21	0	0.129
Lyn <i>et al.</i> (exp. 1995)	1.3×10^4	2.16	0	0.132
Naudascher <i>et al.</i> (exp. 1981)	2.14×10^4	2.10	-	0.130
Taylor and Vezza (2D DVM 1999)	1.06×10^5	2.0	0	-
Koutmos and Mavridis (2D CFD 1997)	2.0×10^4	2.38	0.019	0.1278
Murakami and Mochida (2D CFD 1995)	14285	2.37	-	0.178
Tamura and Kuwahara (2D CFD 1990)	1.0×10^5	2.09	0	0.132
Tamura and Kuwahara (2D CFD 1990)	1.0×10^4	2.4	0	0.103
Tamura and Kuwahara (2D CFD 1990)	1.0×10^4	2.2–2.3	0	0.13

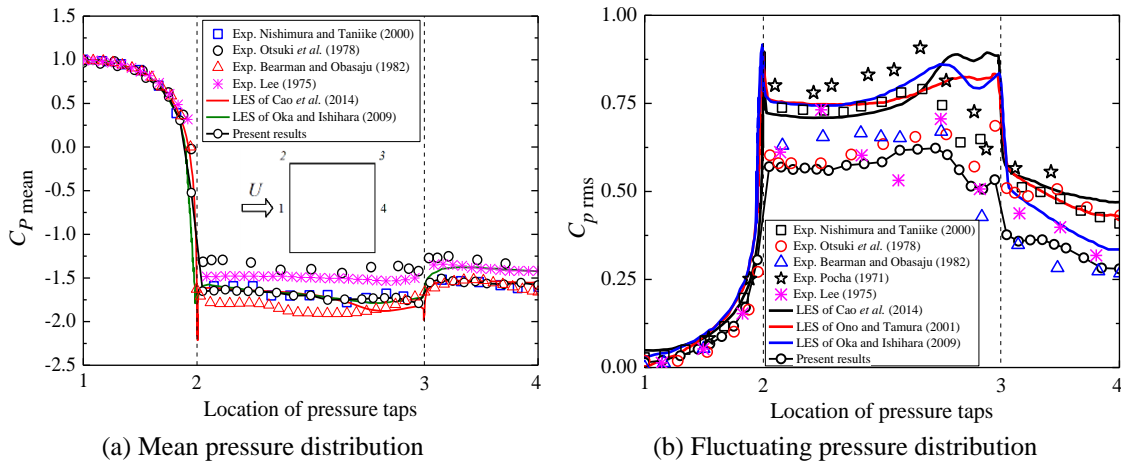


Fig. 6 Wind pressure distributions around a square prism

4.2 Mean drag coefficients

The wind attack angle adopted in this experiment was $\theta = 0^\circ$. Therefore, the separated flow did not reattach to the side surfaces of the square prism. The aerodynamic characteristics of the square prism are independent of Reynolds number. However, the aerodynamic characteristics of the models with corner modifications may be influenced by the Reynolds number. In this section, the Reynolds number effects on the mean drag coefficients of each model are analyzed. Accordingly, 10 models are divided into various categories according to the analysis results.

Fig. 7 shows the variations of mean drag coefficients ($C_{D\ mean}$) for 10 models with various corner modifications in the Reynolds number range between 1.0×10^5 and 4.8×10^5 . For the chamfered-corner models, the mean drag coefficients remain nearly unchanged in the testing

Reynolds number range. The mean drag coefficients of models with $B/D = 5\%$, 10% , and 15% are nearly the same at 1.6–1.7, but are obviously smaller than that of the square prism. However, the rounded-corner models can be classified into 2 categories according to the variations of their mean drag coefficients with the Reynolds number. The mean drag coefficients of the first category (models with $R/D = 0\%$, 5% , 10% , and 15%) remain nearly unchanged in the testing Reynolds number range, and their mean drag coefficient decreases with increasing rounded corner ratio. For the second category (models with $R/D = 20\%$, 30% , and 40%), the mean drag coefficients are obviously influenced by the Reynolds number. Notably, for the model with $R/D = 20\%$, the mean drag coefficient remains nearly unchanged in the Reynolds number range of $1.0 \times 10^5 \leq Re \leq 3.8 \times 10^5$, and then decrease with the increase of Reynolds number from 3.8×10^5 to 4.8×10^5 . For the model with $R/D = 30\%$, the mean drag coefficient remains at a stable value at around 1.1 in the Reynolds number range of $1.0 \times 10^5 \leq Re \leq 2.4 \times 10^5$. Then, a sudden decrease from 1.1 to 0.5 is observed with the increase of Reynolds number from 2.4×10^5 to 2.8×10^5 . For the model with $R/D = 40\%$, the mean drag coefficient remains nearly unchanged in the Reynolds number range of $1.0 \times 10^5 \leq Re \leq 2.1 \times 10^5$. Subsequently, a sudden decrease from 1.0 to 0.7 is found with the increase of Reynolds number from 2.1×10^5 to 2.4×10^5 . Afterwards, the mean drag coefficient slightly decreases to 0.65 with the Reynolds number ranging from 2.4×10^5 to 3.4×10^5 , followed by another sudden decrease with the increase of Reynolds number from 3.4×10^5 to 3.8×10^5 . Finally, the mean drag coefficient remains nearly unchanged in the Reynolds number range of $3.8 \times 10^5 \leq Re \leq 4.8 \times 10^5$.

For the rounded-corner models with $R/D = 30\%$ and 40% , the mean drag coefficients obviously decline in the Reynolds number range of $2.0 \times 10^5 \leq Re \leq 4.0 \times 10^5$. This Reynolds number range corresponds to the variation of the Reynolds number from subcritical range to supercritical range for a circular cylinder. According to the studies by Schewe (1983, 1986), the mean drag coefficient of a circular cylinder also declines rapidly in the critical Reynolds number range ($3 \times 10^5 \leq Re \leq 4 \times 10^5$).

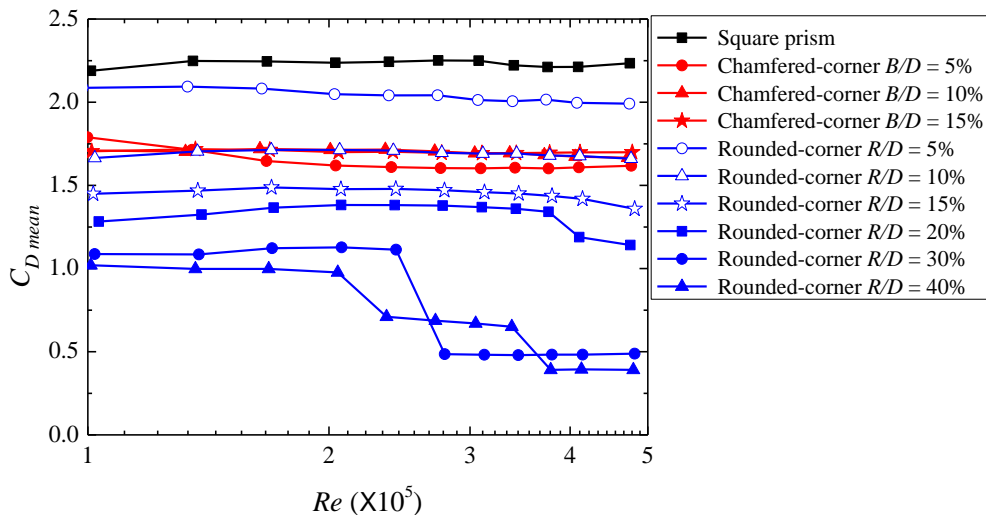


Fig. 7 Variations of mean drag coefficients of 10 models with the Reynolds number

4.3 Wind pressure distributions

According to the variations of the mean drag coefficients of 10 models in the testing Reynolds number range, these models are divided into 3 categories: chamfered-corner models with $B/D \leq 15\%$; rounded-corner models with $R/D \leq 15\%$; and rounded-corner models with $R/D = 20\%$, 30% , and 40% . In this section, the wind pressure distributions on the surface of 10 models are analyzed according to the categorized results.

4.3.1 Chamfered-corner models

Fig. 8 shows the mean pressure distributions around the models with $B/D \leq 15\%$ at $Re \approx 3.4 \times 10^5$. Compared with the square prism, the small chamfered corner ($B/D = 5\%$) obviously decreases the negative pressures on the side surfaces as well as on the leeward side. However, for chamfered-corner models with $B/D = 10\%$ and 15% , the mean pressure coefficients on the side surfaces and the leeward side are between those of the square prism and the chamfered-corner model with $B/D = 5\%$. In addition, for models with $B/D = 10\%$ and 15% , obvious decreases of the mean pressure coefficients are observed on the chamfered corner surfaces near the leading edge (Figs. 8(c) and 8(d)). These decreases could be due to the flow reattachment on the chamfered corner surfaces.

Fig. 9 shows the fluctuating pressure distributions around the models with $B/D \leq 15\%$ at $Re \approx 3.4 \times 10^5$. The fluctuating pressure coefficients on the side surfaces of the square prism are in the range of $0.5\text{--}0.6$ (Fig. 9(a)). Meanwhile, the fluctuating pressure coefficients on the side surfaces of the small chamfered-corner model ($B/D = 5\%$) obviously decreases, and the value range is $0.2\text{--}0.3$ (Fig. 9(b)). For the chamfered-corner models with $B/D = 10\%$ and 15% , the value ranges of fluctuating pressure coefficients on the side surfaces are $0.35\text{--}0.40$ and $0.40\text{--}0.45$, respectively. These value ranges are between those of the square prism and the model with $B/D = 5\%$. In addition, for models with $B/D = 10\%$ and 15% , obvious decreases are observed for fluctuating pressure coefficients on the chamfered corner surfaces near the leading edge. This result also indicates that the flow reattached to the chamfered corner surfaces.

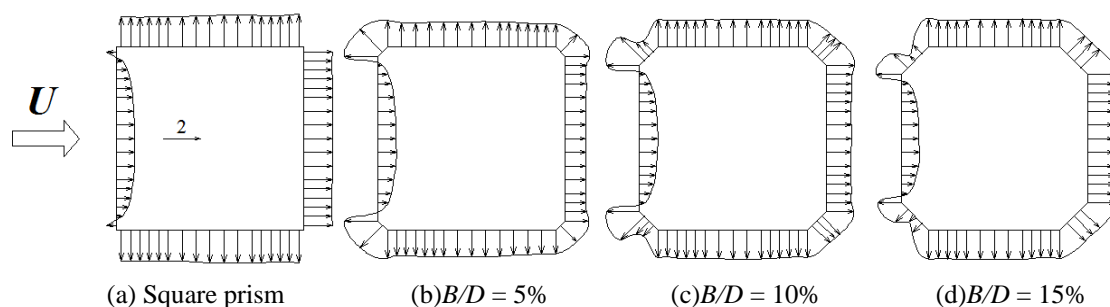
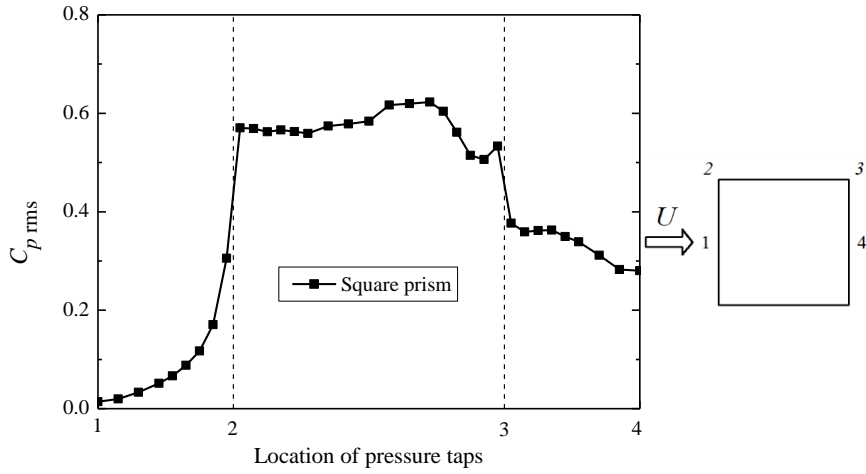
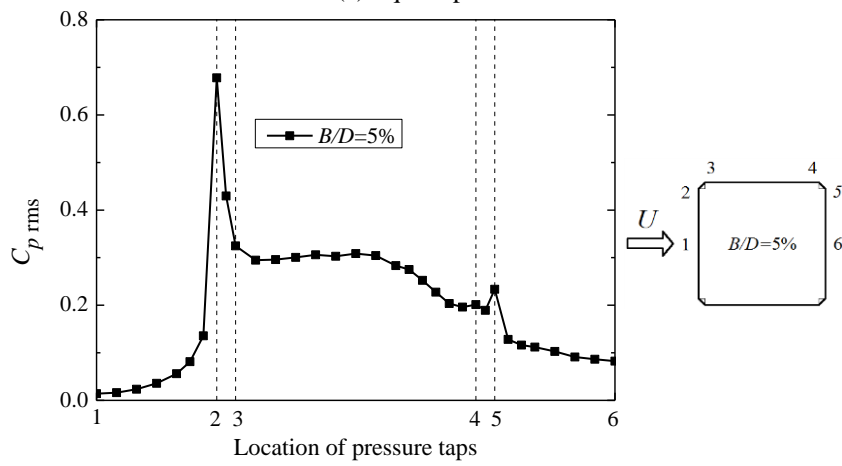


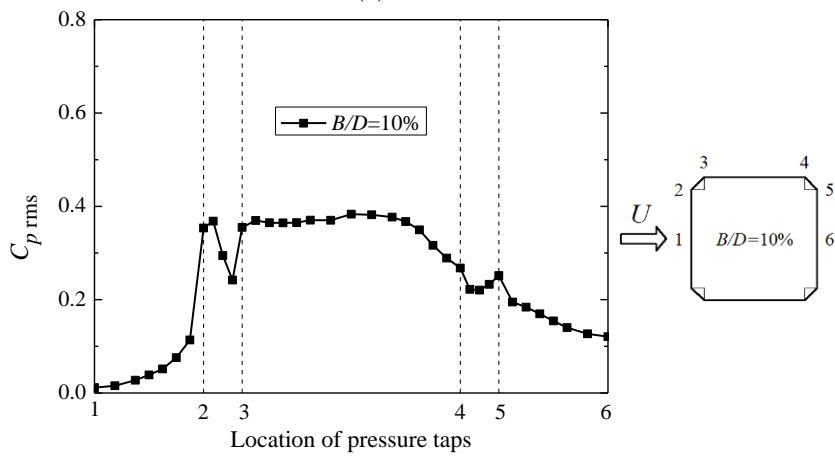
Fig. 8 Mean pressure distributions around chamfered-corner models ($Re \approx 3.4 \times 10^5$)



(a) Square prism



(b) $B/D = 5\%$



(c) $B/D = 10\%$

Continued-

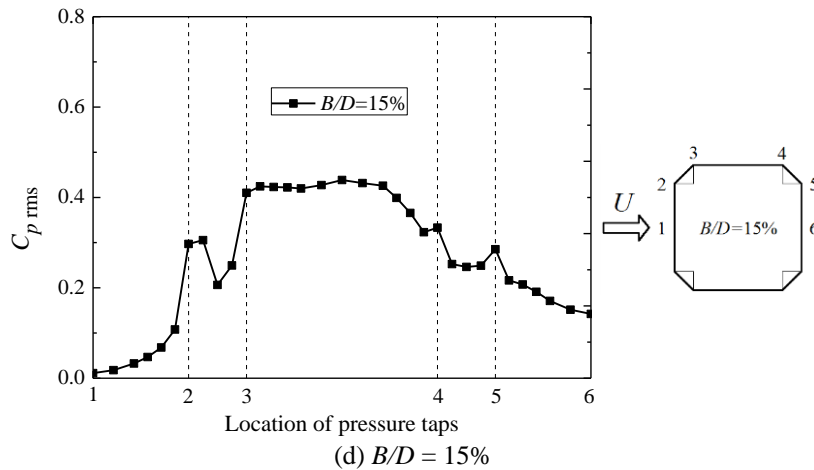


Fig. 9 Fluctuating pressure distributions around chamfered-corner models ($Re \approx 3.4 \times 10^5$)

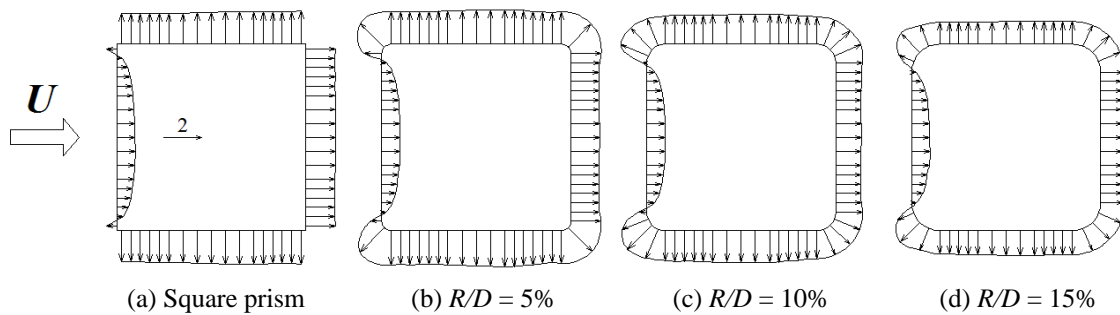


Fig. 10 Mean pressure distributions around rounded-corner models ($Re \approx 3.4 \times 10^5$)

4.3.2 Rounded-corner models with $R/D \leq 15\%$

As discussed in Section 4.2, the aerodynamic characteristics of the rounded-corner models with $R/D \leq 15\%$ are unaffected by the Reynolds number. Fig. 10 shows the mean pressure distributions on the surfaces of the models with $R/D \leq 15\%$ at $Re \approx 3.4 \times 10^5$. For the square prism and the rounded-corner model with $R/D = 5\%$, the mean pressure coefficients on the side surfaces are nearly the same. However, as the rounded corner ratio increases to $R/D = 10\%$ or 15% , the mean pressure coefficients acting on the side surfaces and the leeward side obviously decrease.

Fig. 11 presents the fluctuating pressure coefficients on the surfaces of models with $B/D \leq 15\%$ at $Re \approx 3.4 \times 10^5$. The distribution characteristics are nearly the same for four models, but the values are obviously different. The fluctuating pressure coefficients on the side surface of the square prism are in the range of 0.5–0.6, and slightly increase to around 0.65 when the rounded corner ratio increases to $R/D = 5\%$. For the rounded-corner models with $R/D = 10\%$ and 15% , the fluctuating pressure coefficients acting on the side surfaces are nearly 0.55 and 0.25, respectively.

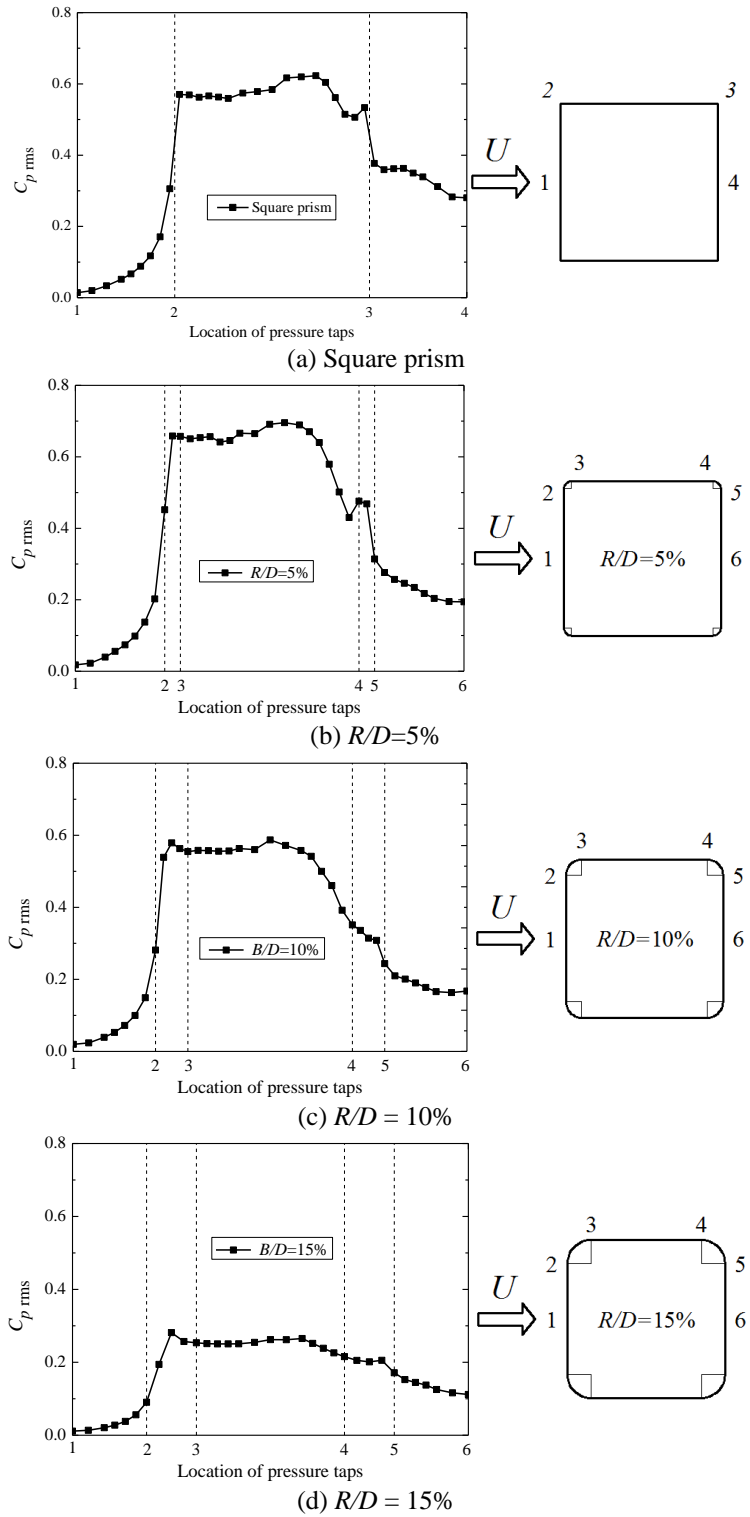


Fig. 11 Fluctuating pressure distributions around rounded-corner models ($Re \approx 3.4 \times 10^5$)

4.3.3 Rounded-corner models with $R/D \geq 20\%$

According to the analysis in Section 4.2, the mean drag coefficients of the models with $R/D=20\%$, 30% , and 40% are obviously influenced by the Reynolds number. Therefore, the Reynolds number effects on the wind pressure distributions around the three models are analyzed in this section. The wind pressure distributions on the surfaces of the models with $R/D=20\%$ and 30% are symmetrical on the streamwise direction, whereas those of the model with $R/D=40\%$ are asymmetrical on the streamwise direction. Figs. 13 and 15 show the fluctuating pressure coefficients acting on the upper half of the model surface for models with $R/D=20\%$ and 30% , respectively. Fig. 17 shows the fluctuating pressure coefficients acting on the entire model surface of the model with $R/D=40\%$.

Fig. 12 shows the mean pressure distributions on the surfaces of the model with $R/D=20\%$. Notably, changes are observed for the case of $Re \approx 4.1 \times 10^5$. Specifically, the mean pressure coefficients on the windward side of the model are unaffected by the Reynolds number, whereas the mean pressure coefficients on the side surfaces for the case of $Re \approx 4.1 \times 10^5$ are obviously different from the other four cases. The separation bubbles shrink toward the leading edges, and the suction near the leading edges increases. The negative pressures acting on the leeward side of the model also decrease. As shown in Fig. 13, the fluctuating pressure distributions acting on the side surface of the model are obviously influenced by the Reynolds number. A gradual decrease of the fluctuating pressure coefficients is also observed with the increase of Reynolds number.

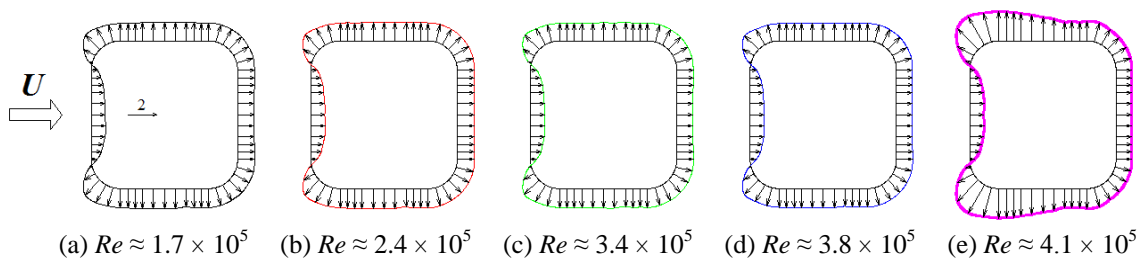


Fig. 12 Mean pressure distributions around the rounded-corner model with $R/D = 20\%$

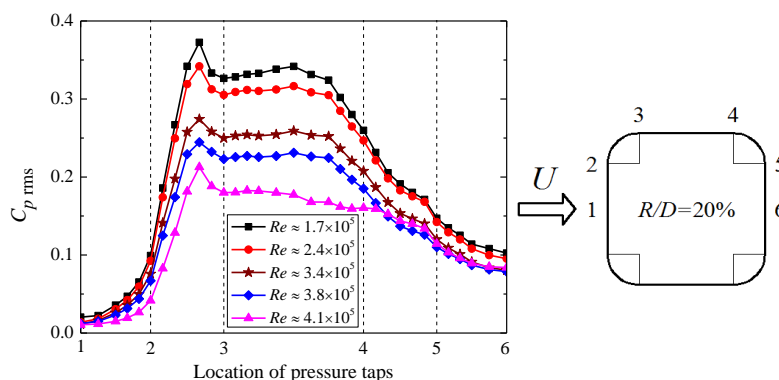


Fig. 13 Fluctuating pressure distributions around the rounded-corner model with $R/D = 20\%$

The mean and fluctuating pressure coefficients acting on the surfaces of the model with $R/D=30\%$ are shown in Figs. 14 and 15, respectively. Two different distributions of the mean pressure coefficients around the model surfaces are observed for five Reynolds numbers. Furthermore, the mean pressure coefficients acting on the side surfaces and the leeward side obviously change with the increase of Reynolds number from $Re \approx 2.4 \times 10^5$ to 3.4×10^5 . The separation bubbles shrink toward the leading edges, and the suction near the leading edges increases. The negative pressures acting on the leeward side of the model also decrease. Correspondingly, the fluctuating pressure coefficients acting on the model surface also show two different distributions for five Reynolds numbers, as shown in Fig. 15. For the cases of $Re \approx 1.7 \times 10^5$ and 2.4×10^5 , the fluctuating pressure distributions around the model surface are nearly the same. Obvious peaks are observed on the rounded corner surfaces near the leading edge, and the large fluctuating pressure coefficients on the side surfaces illustrate that obvious separation bubbles are generated. However, for the cases of $Re \approx 3.4 \times 10^5$, 3.8×10^5 , and 4.1×10^5 , the fluctuating pressure distributions around the model surface are also nearly the same, but obviously differ from those of the first two cases. The peaks on the rounded corner surfaces near the leading edge disappear, but obvious peaks are observed on the rounded corner surfaces near the trailing edge. Therefore, a vortex exists at the rear rounded corner.

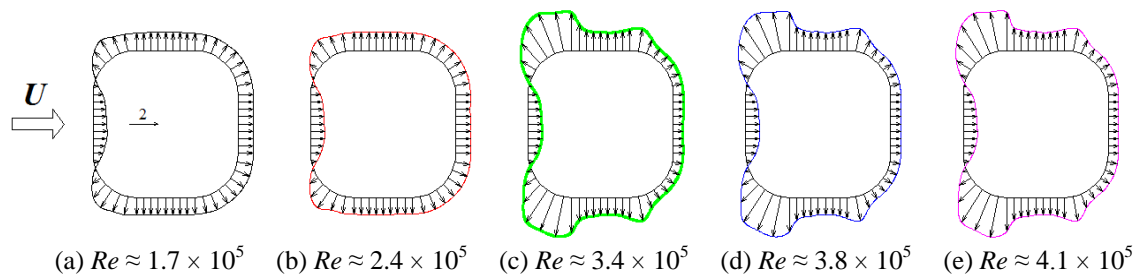


Fig. 14 Mean pressure distributions around the rounded-corner model with $R/D = 30\%$

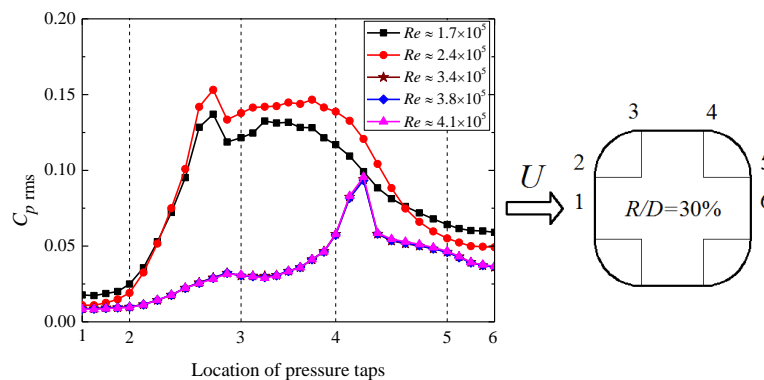


Fig. 15 Fluctuating pressure distributions around the rounded-corner model with $R/D = 30\%$

Fig. 16 shows the Reynolds number effects on the mean pressure distributions on the surfaces of the model with $R/D=40\%$, and three different distributions of mean pressure coefficients are observed. For the case of $Re \approx 1.7 \times 10^5$, the mean pressure distribution on the model surface is symmetrical on the streamwise direction, and the negative pressures acting on the side surfaces of the model are small. However, for the cases of $Re \approx 2.4 \times 10^5$ and 3.4×10^5 , the mean pressure distributions are asymmetrical on the streamwise direction and those acting on the lower surface of the model obviously increase. The negative pressures acting on the rounded corner near the leading edge obviously increase, illustrating that the suction near the leading edges obviously increases. For the cases of $Re \approx 3.8 \times 10^5$ and 4.1×10^5 , the mean pressure distribution on the model surface becomes symmetrical on the streamwise direction again, but obviously differs from the mean pressure distributions at $Re \approx 1.7 \times 10^5$. The negative pressures acting on rounded corner surfaces close to the leading edge obviously increase, demonstrating that the separation bubbles shrink toward the leading edges and the suction near the leading edges increases. Besides, the wake size decreases with the recovery of the base pressure.

The fluctuating pressure distributions around the model surface at various Reynolds numbers are shown in Fig. 17. For the cases of $Re \approx 1.7 \times 10^5$, 2.4×10^5 , and 3.4×10^5 , the fluctuating pressure distributions on the model surface are asymmetrical on the streamwise direction. Notably, an obvious peak is observed at the lower surface of the front rounded corners for the case of $Re \approx 1.7 \times 10^5$. By contrast, obvious peaks appear at the upper surface of the front rounded corners for the cases of $Re \approx 2.4 \times 10^5$ and 3.4×10^5 . Compared with the other cases, the peak value of the fluctuating pressure coefficients is obviously larger for the case of $Re \approx 3.4 \times 10^5$, and another peak is observed on the surfaces of rear rounded corners. For the cases of $Re \approx 3.8 \times 10^5$ and 4.1×10^5 , the fluctuating pressure distributions around the model surface are symmetrical on the streamwise direction, and two small peaks are located at the rear rounded corners.

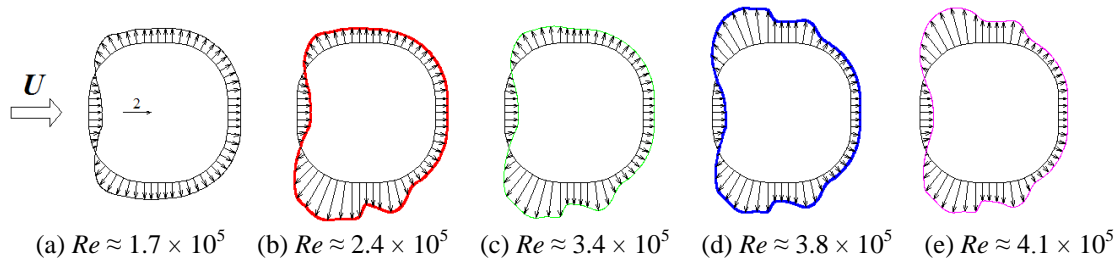


Fig. 16 Mean pressure distributions around the rounded-corner model with $R/D = 40\%$

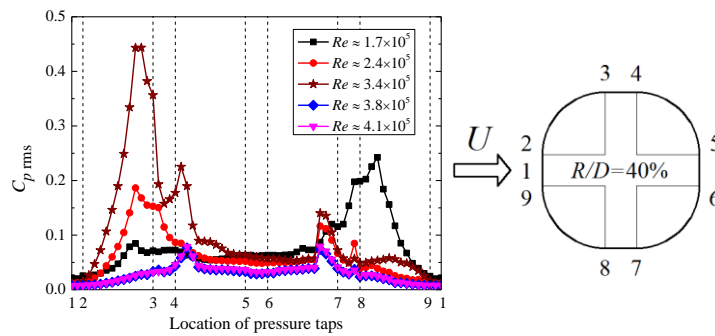


Fig. 17 Fluctuating pressure distributions around the rounded-corner model with $R/D = 40\%$

4.4 Power spectra of aerodynamic force coefficients

4.4.1 Chamfered-corner models

The aerodynamic force coefficients of the models with $B/D \leq 15\%$ and $R/D \leq 15\%$ are unaffected by the Reynolds number. Accordingly, the power spectra of the aerodynamic force coefficients for these models are analyzed at $Re \approx 3.4 \times 10^5$, as shown in Figs. 18 and 19. In Fig. 18(a), for the square prism, an obvious peak on the drag coefficient spectrum curve is observed. This peak corresponds to the reduced frequency of 0.27. For the chamfered-corner model with $B/D=5\%$, no obvious peaks are found on the drag coefficient spectrum curve. For the model with $B/D=10\%$, two obvious peaks are observed on the drag coefficient spectrum curve, and the reduced frequencies corresponding to the two peaks are 0.16 and 0.32. For the model with $B/D=15\%$, only one obvious peak is found on the drag coefficient spectrum curve. In Fig. 18(b), obvious peaks are observed on all power spectrum curves. This observation illustrates that the lift forces acting on these models are produced mostly by vortex shedding in the wake. For the square prism and the model with $B/D=5\%$, the reduced frequencies corresponding to the obvious peaks are very close, and the value range is 0.135–0.140. For models with $B/D=10\%$ and 15% , the reduced frequencies corresponding to the obvious peaks are also very close, and the value is around 0.16.

4.4.2 Rounded-corner models with $R/D \leq 15\%$

Fig. 19 presents the power spectra of the aerodynamic force coefficients for the rounded-corner models with $R/D \leq 15\%$ at $Re \approx 3.4 \times 10^5$. In Fig. 19(a), for models with $R/D=5\%$ and 10% , two obvious peaks are observed on the drag coefficient spectrum curves, and the reduced frequencies corresponding to the peaks are 0.14 and 0.28. For the model with $R/D=15\%$, two peaks are also found on the drag coefficient spectrum curves, but the peaks are not obvious. In Fig. 19(b), obvious peaks are all observed on the lift coefficient spectrum curves for four models. This is similar to the lift coefficient spectrum curves for the chamfered-corner models with $B/D \leq 15\%$.

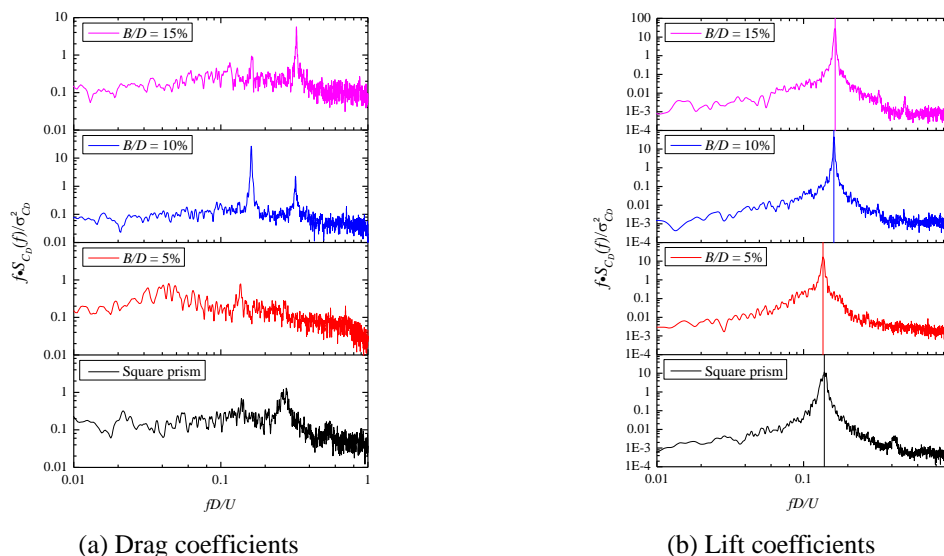


Fig. 18 Power spectra of force coefficients for chamfered-corner models ($Re \approx 3.4 \times 10^5$)

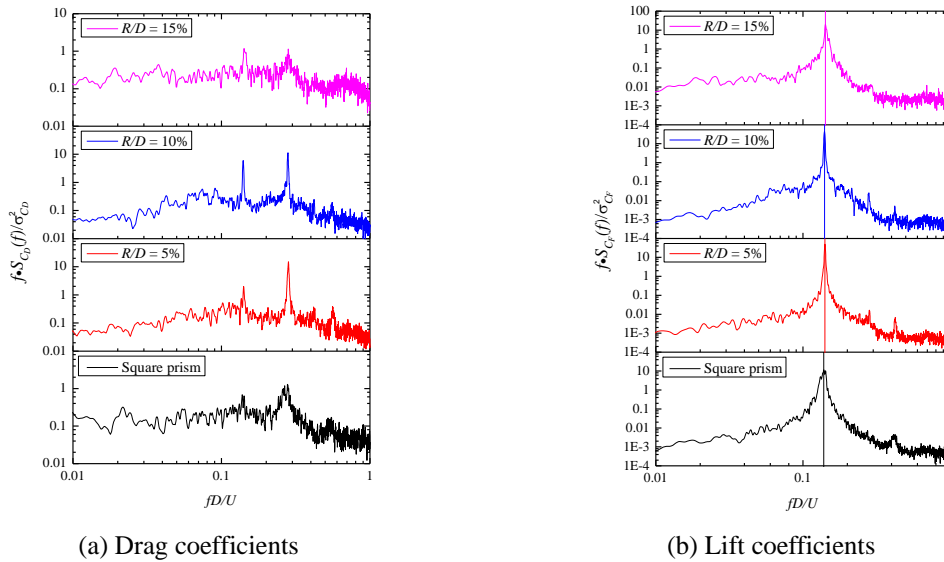


Fig. 19 Power spectra of force coefficients for rounded-corner models with $R/D \leq 15\%$ ($Re \approx 3.4 \times 10^5$)

However, the obvious difference between Figs. 18(b) and 19(b) is that the reduced frequencies corresponding to the obvious peak in Fig. 19(b) remain nearly unchanged for four models, and the value range is 0.135–0.145.

4.4.3 Rounded-corner models with $R/D=20\%$, 30% , and 40%

For the models with $R/D=20\%$, 30% , and 40% , the variation of their lift coefficient power spectra with the Reynolds number are presented in Fig. 20. For the model with $R/D=20\%$ (Fig. 20(a)), the power spectra of the lift coefficients does not change in the Reynolds number range of $1.0 \times 10^5 \leq Re \leq 3.8 \times 10^5$, and only one peak at the reduced frequency of $f \cdot D/U \approx 0.155$ is observed. However, significant changes are observed when the Reynolds number reaches $Re \approx 4.1 \times 10^5$, and the spectrum curve changes from one peak to double peaks. For the model with $R/D=30\%$ (Fig. 20(b)), two different distributions for the lift coefficient spectrum curves are observed for five Reynolds number cases. For the cases of $Re \approx 1.7 \times 10^5$ and 2.4×10^5 , two peaks are found on the power spectrum curves and the reduced frequency corresponding to this peak is $f \cdot D/U \approx 0.35$. For the model with $R/D=40\%$ (Fig. 20(c)), the variations of the power spectra of lift coefficients with the Reynolds numbers are comparatively complex. For the cases of $Re \approx 1.7 \times 10^5$ and 2.4×10^5 , obvious peaks are observed on the power spectrum curves and the reduced frequencies corresponding to these peaks are 0.18 and 0.30. However, the peaks disappear for the case of $Re \approx 3.4 \times 10^5$. As the Reynolds number increases to $Re \approx 3.8 \times 10^5$ and 4.1×10^5 , obvious peaks on the power spectrum curves are observed again, and the reduced frequencies corresponding to the peaks are nearly the same at 0.38.

4.5 Strouhal number

The frequency domain features of fluctuating forces can be revealed by the power spectrum analysis. The vortex shedding frequency can also be obtained by analyzing the power spectrum of

lift coefficients. The Strouhal number is defined as the reduced frequency corresponding to the obvious peak on the lift coefficient spectrum curve (Liang *et al.* 2002). For seven models with $B/D \leq 15\%$ and $R/D \leq 15\%$, their Strouhal numbers are unaffected by the Reynolds number. Fig. 21 shows the variations of the Strouhal numbers with chamfered corner ratio or rounded corner ratio at $Re \approx 3.4 \times 10^5$. For the rounded-corner models with $R/D \leq 15\%$, the Strouhal numbers remain nearly unchanged at 0.135–0.145. However, for the chamfered-corner models with $B/D \leq 15\%$, the Strouhal numbers obviously vary with the chamfered corner ratio. Notably, the Strouhal numbers of the models with $B/D = 5\%$ and 10% are very close, and the value range is 0.135–0.140. Meanwhile, the Strouhal numbers of the models with $B/D = 10\%$ and 15% significantly increase, and the value range is 0.160–0.165.

For the rounded-corner models with $R/D = 20\%$, 30% , and 40% , the variations of their Strouhal numbers with the Reynolds numbers are presented in Fig. 22. For the model with $R/D = 20\%$, the Strouhal number remains at a stable value of around 0.15 in the Reynolds number range of $1.0 \times 10^5 \leq Re \leq 3.8 \times 10^5$. Then, a slight decrease is observed with the increase of Reynolds number from 3.8×10^5 to 4.1×10^5 . For the models with $R/D = 30\%$ and 40% , sudden increases of the Strouhal numbers are observed in the testing Reynolds number range. Notably, the Strouhal number of the model with $R/D = 30\%$ significantly increases from 0.16 to 0.35 with the increase of Reynolds number from $Re \approx 2.4 \times 10^5$ to $Re \approx 2.8 \times 10^5$. For the model with $R/D = 40\%$, the Strouhal number slightly decrease with the increase of Reynolds number from 1.0×10^5 to 2.1×10^5 . Subsequently, a suddenly increase from 0.18 to 0.30 is found with the increase of Reynolds number from $Re \approx 2.1 \times 10^5$ to $Re \approx 2.4 \times 10^5$. Furthermore, in the Reynolds number range of $2.7 \times 10^5 \leq Re \leq 3.4 \times 10^5$, no obvious peaks on the lift coefficient spectrum curves are found. In the Reynolds number range of $3.8 \times 10^5 \leq Re \leq 4.8 \times 10^5$, obvious peaks on the lift coefficient spectrum curves are observed again. The Strouhal number also remains at a stable value of nearly 0.38.

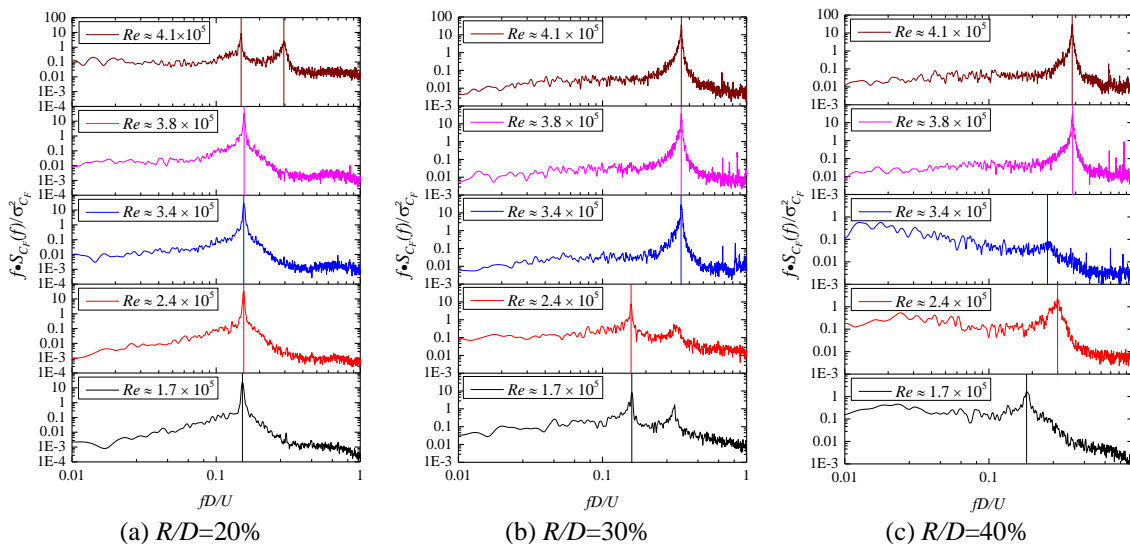


Fig. 20 Power spectra of lift coefficients for rounded-corner models with $R/D \geq 20\%$

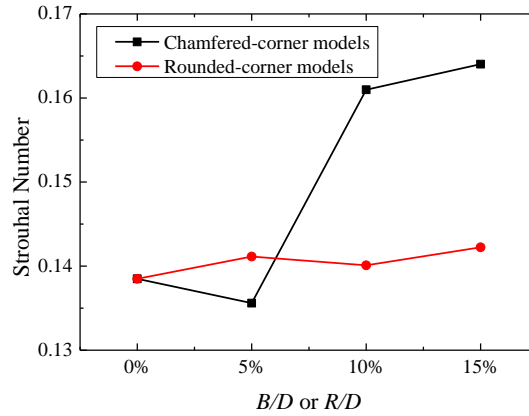


Fig. 21 Strouhal numbers of seven models with $B/D \leq 15\%$ and $R/D \leq 15\%$ ($Re \approx 3.4 \times 10^5$)

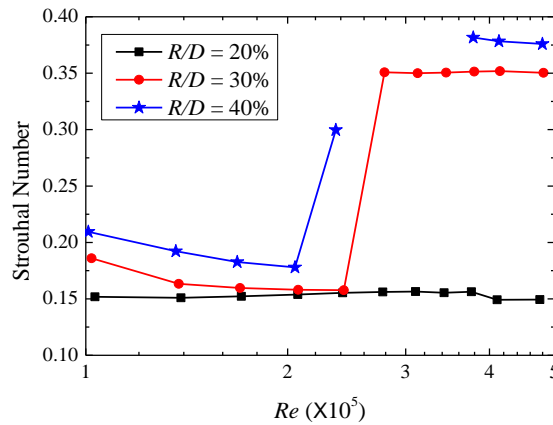


Fig. 22 Strouhal numbers of rounded-corner models with $R/D = 20\%$, 30% and 40%

In the Reynolds number range of $2.0 \times 10^5 \leq Re \leq 4.0 \times 10^5$, obvious jumps in the Strouhal number are observed for the rounded-corner models with $R/D = 30\%$ and 40% . This trend is similar to the variations of the Strouhal numbers of a circular cylinder in the critical Reynolds number range of $3 \times 10^5 \leq Re \leq 4 \times 10^5$ (Schewe 1983, 1986).

5. Conclusions

Wind pressure measurements were conducted to investigate the effects of corner modifications on the aerodynamic characteristics of a 2D square prism in uniform flow with low turbulence level, and the Reynolds number varied from 1.0×10^5 to 4.8×10^5 . Wind pressure distributions, drag coefficients, power spectra of aerodynamic force coefficients, and Strouhal numbers are analyzed. The mean drag coefficients of the chamfered-corner models with $B/D \leq 15\%$ and the rounded-corner models with $R/D \leq 15\%$ are unaffected by the Reynolds number. On the contrary,

the mean drag coefficients of the rounded-corner models with $R/D = 20\%$, 30% , and 40% are obviously influenced by the Reynolds number.

For the four chamfered-corner models ($B/D = 0\%$, 5% , 10% , and 15%), their aerodynamic characteristics are unaffected by the Reynolds number. In addition, the chamfered corner ratios of $B/D = 10\%$ and 15% can produce the flow reattachment on the surfaces of front chamfered corners. The Strouhal numbers of the models with $B/D = 10\%$ and 15% are significantly larger than those of the models with $B/D = 5\%$ and 10% . For the four rounded-corner models with $R/D = 0\%$, 5% , 10% , and 15% , their mean drag coefficient decreases with increasing rounded corner ratio, and their Strouhal numbers remain nearly unchanged at $0.135\text{--}0.145$.

For the rounded-corner models with $R/D = 20\%$, 30% , and 40% , their aerodynamic characteristics are obviously influenced by the Reynolds number. For the rounded-corner models with $R/D = 20\%$ and 30% , two flow regimes around the model are found in the testing Reynolds number range. However, for the rounded-corner model with $R/D = 40\%$, three flow regimes around the model are observed in the testing Reynolds number range, and the transitions between the three regimes are governed by the Reynolds number. In the testing Reynolds number range, the Strouhal number of the rounded-corner model with $R/D = 20\%$ remains nearly unchanged. By contrast, sudden jumps of the Strouhal numbers are observed for the rounded-corner models with $R/D = 30\%$ and 40% . The variations of the Strouhal numbers for the models with $R/D = 20\%$, 30% , and 40% correspond to the transitions of the flow regimes around the model.

Acknowledgments

The authors gratefully acknowledge the supports from the National Natural Science Foundation of China (91215302, 90715040) and Key project of State Key Lab. of Disaster Reduction in Civil Eng. (SLDRCE15-A-04).

References

- Bearman, P.W. and Obasaju, E.D. (1982), "An experimental study of pressure fluctuations on fixed and oscillating square-section cylinders", *J. Fluid Mech.*, **119**, 297-321.
- Bosch, G. and Rodi, W. (1998), "Simulation of vortex shedding past a square cylinder with different turbulence models", *Int. J. Numer. Meth. Fl.*, **28**(4), 601-616.
- Cao, S., Zhou, Q. and Zhou, Z. (2014), "Velocity shear flow over rectangular cylinders with different side ratios", *Comput. Fluids.*, **96**, 35-46.
- Carassale, L., Freda, A. and Marrè-Brunenghi, M. (2013), "Effects of free-stream turbulence and corner shape on the galloping instability of square cylinders", *J. Wind Eng. Ind. Aerod.*, **123**, 274-280.
- Carassale, L., Freda, A. and Marrè-Brunenghi, M. (2014), "Experimental investigation on the aerodynamic behavior of square cylinders with rounded corners", *J. Fluid. Struct.*, **44**, 195-204.
- Choi, C.K. and Kwon, D.K. (2003), "Effects of corner cuts and angles of attack on the Strouhal number of rectangular cylinders", *Wind Struct.*, **6**(2), 127-140.
- Gu, M. and Quan, Y. (2004), "Across-wind loads of typical tall buildings", *J. Wind Eng. Ind. Aerod.*, **92**(13), 1147-1165.
- Hayashida, H. and Iwasa, Y. (1990), "Aerodynamic shape effects of tall building for vortex induced Vibration", *J. Wind Eng. Ind. Aerod.*, **33**(1), 237-242.
- Huang, R.F., Lin, B.H. and Yen, S.C. (2010), "Time-averaged topological flow patterns and their influence

- on vortex shedding of a square cylinder in crossflow at incidence”, *J. Fluid. Struct.*, **26**(3), 406-429.
- Huang, R.F. and Lin, B.H. (2011), “Effects of flow patterns on aerodynamic forces of a square cylinder at incidence”, *J. Mech.*, **27**(3), 347-355.
- Igarashi, T. (1984), “Characteristics of the flow around a square prism”, *Bull. JSME*, **27**(231), 1858-1865.
- Knisely, C.W. (1990), “Strouhal numbers of rectangular cylinders at incidence: a review and new data”, *J. Fluid. Struct.*, **4**(4), 371-393.
- Koutmos, P. and Mavridis, C. (1997), “A computational investigation of unsteady separated flows”, *Int. J. Heat Fluid Fl.*, **18**(3), 297-306.
- Kwok, K.C.S. (1988), “Effect of building shape on wind-induced response of tall building”, *J. Wind Eng. Ind. Aerod.*, **28**(1), 381-390.
- Lee, B.E. (1975), “The effect of turbulence on the surface pressure field of a square prism”, *J. Fluid Mech.*, **69**(2), 263-282.
- Liang, S.G., Liu, S.C., Li, Q.S., Zhang, L.L. and Gu, M. (2002), “Mathematical model of across wind dynamic loads on rectangular tall buildings”, *J. Wind Eng. Ind. Aerod.*, **90**(12), 1757-1770.
- Lyn, D.A., Einav, S., Rodi, W. and Park, J.H. (1995), “A laser-Doppler velocimetry study of ensemble-averaged characteristics of the turbulent near wake of a square cylinder”, *J. Fluid Mech.*, **304**, 285-319.
- Miyashita, K., Katagiri, J., Nakamura, O., Ohkuma, T., Tamura, Y., Itoh, M. and Mimachi, T. (1993), “Wind-induced response of high-rise buildings Effects of corner cuts or openings in square buildings”, *J. Wind Eng. Ind. Aerod.*, **50**, 319-328.
- Murakami, S. and Mochida, A. (1995), “On turbulent vortex shedding flow past 2D square cylinder predicted by CFD”, *J. Wind Eng. Ind. Aerod.*, **54**, 191-211.
- Nakamura, Y. and Ohya, Y. (1984), “The effects of turbulence on the mean flow past two-dimensional rectangular cylinders”, *J. Fluid Mech.*, **149**, 255-273.
- Nakamura, Y. and Ozono, S. (1987), “The effects of turbulence on a separated and reattaching flow”, *J. Fluid Mech.*, **178**, 477-490.
- Naudascher, E., Weske, J.R. and Fey, B. (1981), “Exploratory study on damping of galloping vibrations”, *J. Wind Eng. Ind. Aerod.*, **8**(1), 211-222.
- Nishimura, A. and Taniike, Y. (2000), “Fluctuating wind forces of a stationary two dim. square prism” (in Japanese), *Proceedings of the 16th National Symposium on Wind Engineering*, Tokyo, Japan.
- Norberg, C. (1993), “Flow around rectangular cylinders: pressure forces and wake frequencies”, *J. Wind Eng. Ind. Aerod.*, **49**(1), 187-196.
- Okajima, A. (1982), “Strouhal numbers of rectangular cylinders”, *J. Fluid Mech.*, **123**, 379-398.
- Okajima, A. (1990), “Numerical simulation of flow around rectangular cylinders”, *J. Wind Eng. Ind. Aerod.*, **33**(1), 171-180.
- Oka, S. and Ishihara, T. (2009), “Numerical study of aerodynamic characteristics of a square prism in a uniform flow”, *J. Wind Eng. Ind. Aerod.*, **97**(11), 548-559.
- Ono, Y. and Tamura, T. (2001), “Numerical study for turbulent effect on aerodynamics of a square cylinder”, *Proceedings of the 5th Asia-Pacific Conference on Wind Engineering*, Kyoto, Japan, October.
- Otsuki, Y., Fujii, K., Washizu, K.T. and Ohya, A. (1978), “Wind tunnel experiments on aerodynamic forces and pressure distributions of rectangular cylinders in a uniform flow”(in Japanese), *Proceedings of the Fifth Symposium on Wind Effects on Structures*, Tokyo, Japan.
- Pocha, J.J. (1971), “On unsteady flow past cylinders of square cross-section”, Ph.D. Dissertation, University of London, London.
- Schewe, G. (1983), “On the force fluctuations acting on a circular cylinder in crossflow from subcritical up to transcritical Reynolds numbers”, *J. Fluid Mech.*, **133**, 265-285.
- Schewe, G. (1986), “Sensitivity of transition phenomena to small perturbations in flow round a circular cylinder”, *J. Fluid Mech.*, **172**, 33-46.
- Shimada, K. and Ishihara, T. (2002), “Application of a modified $k-\epsilon$ model to the prediction of aerodynamic characteristics of rectangular cross-section cylinders”, *J. Fluid. Struct.*, **16**(4), 465-485.

- Sohankar, A., Davidson, L. and Norberg, C. (2000), "Large eddy simulation of flow past a square cylinder: Comparison of different subgrid scale models", *J. Fluid. Eng.- T. ASME*, **122**(1), 39-47.
- Tamura, T. and Kuwahara, K. (1990), "Numerical study of aerodynamic behavior of a square cylinder", *J. Wind Eng. Ind. Aerod.*, **33**(1), 161-170.
- Tamura, T. and Miyagi, T. (1999), "The effect of turbulence on aerodynamic forces on a square cylinder with various corner shapes", *J. Wind Eng. Ind. Aerod.*, **83**(1), 135-145.
- Tamura, T., Miyagi, T. and Kitagishi, T. (1998), "Numerical prediction of unsteady pressures on a square cylinder with various corner shapes", *J. Wind Eng. Ind. Aerod.*, **74**, 531-542.
- Tamura, T., Ohta, I. and Kuwahara, K. (1990), "On the reliability of two-dimensional simulation for unsteady flows around a cylinder-type structure", *J. Wind Eng. Ind. Aerod.*, **35**, 275-298.
- Taylor, I. and Vezza, M. (1999), "Prediction of unsteady flow around square and rectangular section cylinders using a discrete vortex method", *J. Wind Eng. Ind. Aerod.*, **82**(1), 247-269.
- Vickery, B.J. (1966), "Fluctuating lift and drag on a long cylinder of square cross-section in a smooth and in a turbulent stream", *J. Fluid Mech.*, **25**(3), 481-494.
- Wang, J.M., Cheng, C.M. and Tens, P.T. (2003), "Design wind loads on tall buildings: a wind tunnel data based expert system approach", *Proceedings of 11th International Conference on Wind Engineering*. Lubbock, TX, USA.
- Wang, X. and Gu, M. (2015), "Experimental investigation of Reynolds number effects on 2D rectangular prisms with various side ratios and rounded corners", *Wind Struct.*, **21**(2), 183-202.
- Yen, S.C. and Yang, C.W. (2011), "Flow patterns and vortex shedding behavior behind a square cylinder", *J. Wind Eng. Ind. Aerod.*, **99**(8), 868-878.
- Yu, D.H. and Kareem, A. (1996), "Two-dimensional simulation of flow around rectangular prisms", *J. Wind Eng. Ind. Aerod.*, **62**(2), 131-161.
- Yu, D.H. and Kareem, A. (1997), "Numerical simulation of flow around rectangular prism", *J. Wind Eng. Ind. Aerod.*, **67**, 195-208.